Breast Cancer Diagnosis from Histopathology Images Using Deep Learning Methods: A Survey

Vivek Patel[1*], *Vijayshri* Chaurasia[1], *Rajesh* Mahadeva[2,3*], *Abhijeet* Ghosh[4], *Saurav* Dixit[5], *Bhivraj* Suthar[2], *Vinay* Gupta[2], *D.* Siri[6], *Y Jeevan Nagendra* Kumar[6], *Navdeep* Dhaliwal[7], *Harikrishna* Bommala[8] and *Kaushal* Kumar[9]

[1]Maulana Azad National Institute of Technology, Bhopal, Madhya Pradesh, 462003, India
[2]Khalifa University of Science and Technology, Abu Dhabi, 127788, United Arab Emirates
[3]Division of Research and Innovation, Uttaranchal University, Dehradun, 248012, India
[4]Amity Institute of English Studies and Research, Amity University, Patna, Bihar, 801503, India
[5]Peter the Great St Petersburg Polytechnic University, St Petersburg, 195251, Russia
[6]GRIET, Bachupally, Hyderabad, Telangana, 500090, India
[7]Lovely Professional University, Phagwara, Punjab, 144001, India
[8]K G Reddy College of Engineering & Technology, Hyderabad, Telangana, 501504, India
[9]K R Mangalam University, Gurgaon, Haryana, 122103, India

Abstract. Breast cancer is a major public health issue that may be remedied with early identification and efficient organ therapy. The diagnosis and prognosis of severe and serious illnesses are likely to be followed and examined by a biopsy of the affected organ in order to identify and classify the malignin cells or tissues. The histopathology of tissue is one of the major advancements in modern medicine for the identification of breast cancer. Haematoxylin and eosin staining slides are used by pathologists to identify benign or malignant tissue in clinical instances of invasive breast cancer. A digital whole slide imaging (WSI) is a high-resolution digital file that is permanently stored in memory for flexible use. This article will look at and compare how breast cancer cells are categorised manually and automatically. lobular carcinoma in situ and ductal carcinoma in situ are the two types of breast cancer. Here, detailed explanations of numerous techniques utilised in histopathology pictures for nucleus recognition, segmentation, feature extraction, and classification are given. The pre-processed image is utilised to extract the nucleus patch using several feature extraction approaches. Thanks to the great computational capability of the general processing unit (GPU), algorithms may be implemented effectively and efficiently. Deep Convolution Neural Network (DCNN), Support Vector Machines (SVM), and other machine learning methods are the most popular and effective computer algorithms.

Keywords: Deep Learning; Transfer learning; Breast cancer Diagnosis; Histopathology Image; Cross-level attention, Convolutional Neural Network.

1 Introduction

A major problem for women's health worldwide is breast cancer. Based on GLOBOCAN 2012 data, the standardized incidence rate (ASR) for invasive breast cancer (females) was 29.1 per 100,000 women per year in Asia, which is almost 30% of the population in the West [1, 2]. ASR per 100,000 women per year is 91.6 in North America and 71.1 in Europe WHO reported 2.09 million cases and 627,000 deaths worldwide due to breast cancer alone [2, 9]. This represents the incidence and mortality rates by race and ethnicity at that time. Invasive

* Corresponding author: vivekpatel.iet46@gmail.com

breast cancer and ductal carcinoma in situ (DCIS) incidence rates both increased significantly between the 1980s and 1990s. In the USA alone, 41,760 women will lose their lives to breast cancer in 2019 [1, 2, 8, 9].

Hungarian and Russian pathologists and surgeons created and implemented the Interactive Histopathology Consultation Network (INTERPATH) initiative to conduct site-experimental casting of histological and cytological multimedia materials between hospitals and university institutes of pathology [3, 4]. A biopsy of the affected organ is necessary for the diagnosis and prognosis of the majority of serious illnesses in order to measure and recognize the deformation of cells (cytology) or tissues (histology) in comparison to normal cells [5].

The creation of potent computer-assisted analytical methods for the interpretation of radiological data has been made possible over the past ten years because to huge advances in processing power and advancements in image analysis techniques [8]. The ability to digitize and save tissue histology slides as digital images has been made possible by the development of whole slide imaging (WSI) [4 -9]. A full microscope slide is scanned using WSI, which is often referred to as virtual microscopy, to produce a single high-resolution digital file. Histopathologists have frequently been at the forefront of computer literacy in the field of diagnostics since pathology is one of the most computer-intensive medical screening fields [6-10]. The FDA authorized digital imaging in 2011, making it the most common, sensitive, and widely used imaging technology to date. The most popular and practical method for helping the pathologist preserve slides digitally so they may be utilized for image analysis in the future is called digital whole slide imaging (DWSI) [7-12].

The numerous specialized systems for breast cancer histopathologic categorization now in use are descriptive and based on the histology, cytological, or both, of the tumors [28]. Screening is crucial for early identification of breast cancer since it usually has no symptoms when the tumor is small and manageable [1, 5]. Four categories of tumor exist: (2) Other (rare) Tumors (1) Lobular Carcinoma (3) Infiltrating Carcinoma (4) Carcinoma with High Metastasis. The WHO approach includes a categorization for tumors that is grade-based and is based on the advice offered by Bloom and Richardson. This is determined by the number of hyperchromatic mitoses and nuclei per high spectral vision (1, 2 or 3 points: few, moderate, many), irregular nuclei in terms of size, shape, and staining, and irregular nuclei in terms of tubule formation. The sum of these points is graded as I for points 3-5, II for points 6-7, and III for points 8–9 [6-13, 28].

1.1 Fluorescent microscopic imaging methods

A breakthrough in optical imaging occurred during the past 20 years, and several imaging techniques are now accessible and in use. The findings for personal identification were more precise using polarization difference imaging [5-8]. The two polarization components' peak intensities vary depending on the tissue type and illumination wavelength [2].

- The Fourier Transform-Infrared (FT-IR) imaging technique performs molecular-level spectroscopic investigation. In the study and diagnosis of breast cancer, optical imaging plays a significant role [4].

- Pathologists further departed from the subjective assessment of morphological patterns with the introduction of multispectral imaging, which marked a turning point in the area of cancer and other illness diagnostics [5].

- The near infrared (NIR) autofluorescence pictures have been utilized to identify and photograph the cancer in real time, whereas usually, cancer diagnosis is made

through a screening procedure in which biopsy tissue is examined under a microscope by a skilled pathologist [6, 7].

Table 1. India and USA breast cancer age-wise patients' distribution with individual percentage and number of patients.

India (2062 Patients)			USA (48,100 Patients)		
Age group	**Number**	**Percentage**	**Age group**	**Number**	**Percentage**
< 30	63	03.10%	< 40	1,180	02.00%
31-40	348	16.90%	40-49	8,130	17.00%
41-50	645	31.30%	50-59	12,730	26.00%
51-60	569	27.60%	60-69	14,460	30.00%
61-70	317	15.40%	70-79	8,770	18.00%
>70	120	05.80%	>80	2,830	06.00%

Using a straightforward Bayesian classifier based on 8 extracted features and complete-leave-one-out cross-validation, this strategy is able to achieve a high degree of classification accuracy (98%) in the classification of 64 photos (n=64) [7]. According to the 2019 study, table-I below displays the age-wise percentage of female patients from India and the USA who are dealing with the disease of breast cancer. Table 1 shows that women between the ages of 40 and 60 are those most affected by breast cancer.

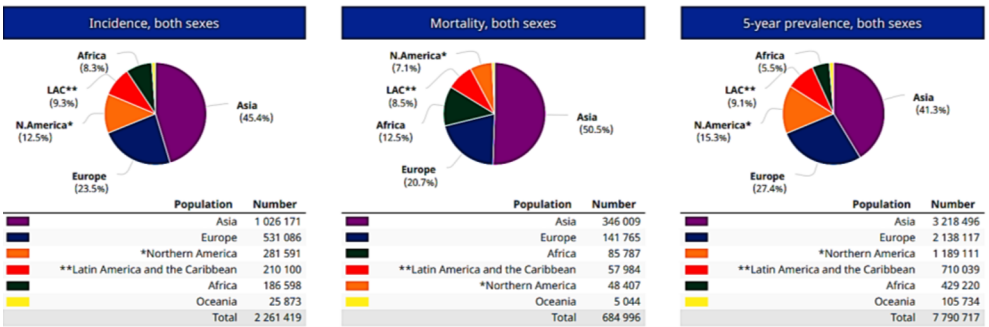

Fig. 1. Breast cancer report as per world health organization (WHO) year2023 [2].

2 Breast Cancer diagnosis methods

The pathological procedure of H&E staining is used to emphasize the tissue's structure. To improve the spectral clarity of a picture, paraffin is mixed with the tissue prior to H&E staining [4, 5]. Since the previous decade, the DWSI has made it easier for the pathologist to preserve the tissue pictures and utilize them to identify tissue structural deformation [4, 6, 7-8]. An enhanced staining method called immunohistochemistry (IHC) uses antibodies to draw attention to certain antigens that are present in the tissue seen in Fig. 2(b) and (c) [19]. IHC is frequently used in breast cancer to highlight the presence of the hormone receptors for estrogen, progesterone, and human epidermal growth factor 2 (HER2) as well as to assess the tumor's growth, for instance by highlighting the protein Ki-67, which is linked to cell growth [18].

The identification of cell nuclei for diagnostic reasons is a crucial component of many laboratory tests used in medicine [5, 7, 10, 20-35]. Correct diagnosis and automated microscopy applications, such as cell counting and tissue architecture analysis, can both

benefit from the precise placement of cell nuclei [12]. Histopathology and image processing are the two main subfields of biomedical imaging [21]. The many constituent pieces of the overall structure of histopathological imaging are depicted in Fig. 3.

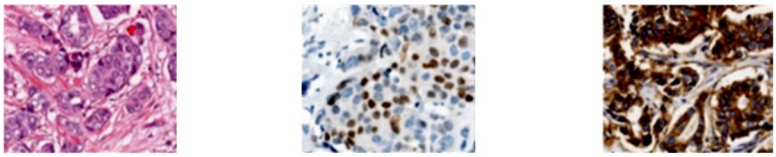

(a) (b) (c)

Fig. 2. Breast cancer histopathology images (a) is H&E based (b) is IHC based and (c) is mixture staining (IHC then H&E) [19].

The findings were carefully evaluated across 25 typical photos, encompassing more than 7400 nuclei, using the most common approach, nuclear segmentation (15 in vitro images and 10 in vivo images) [12-14]. The suggested segmentation algorithm's total accuracy is close to 86%. The accuracy was determined to be more than 94% when just over- and under-segmentation faults were taken into account [10]. For stained picture I [18], the H&E staining may be statistically modelled in Eqn. (1).

$$I = (C, \psi) \text{ and } \psi_{new} = \exp(-S\psi) \quad (1)$$

If C is the pixel linked with the color space, S is the stain matrix, and ψ_{new} is the RGB color space. Again, we write $\psi_{new}(c) = D\varphi(c)$ *where* $D = S^{-1}$ and color deconvolution D, and optical density φ is represented as in Eqn. (2).

$$\varphi(c) = -\log(\psi(c)) \quad (2)$$

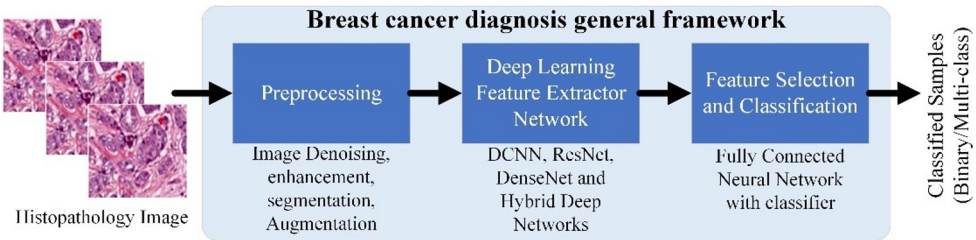

Fig. 3 Breast cancer diagnosis generalized steps and framework for computer aided diagnosis (CAD) of cancer.

3 Preprocessing steps of an image

3.1 Thresholding

This technique converts an image's intensity level into a binary image I by giving each pixel a value of one or zero depending on whether its intensity is above or below a predetermined global thresholding T (3) [18].

$$I = \begin{cases} 1, \textit{ if } I(i) \geq 1 \\ 0, \textit{ otherwise} \end{cases} \quad (3)$$

Use of computational techniques like the Otsu approach with minimal intraclass variation may be used to determine the threshold value (T) for optimum thresholding.

3.2 Morphology

Based on a set-theoretic approach, morphology treats images as the components of a set. The foreground pixel and structural component are denoted by P_f and S, respectively [20, 25, 27].

$$\begin{aligned} &Erosion: P_f \square \qquad \forall s \in S,\ x+s \in P_f\} \\ &Dilation: P_f \oplus S = \{x+s \mid x \in I \wedge s \in S\}. \end{aligned} \tag{4}$$

Where □ are the erosion and dilation (morphological operators) shown in Eqn. (4). Between picture I and it's opening as, there is a difference caused by the white top-hat transform.

$$T_w\ (I) = P_f\ - [P_f \square \tag{5}$$

The difference between picture I and its close as-is is represented by the black top-hat transform shown in Eqn. (6).

$$T_b\ (I) = P_f\ - [P_f \oplus S]\square \tag{6}$$

Level sets and Active Contour Models: Active contour models (ACMs), often referred to as deformable models, are frequently employed in picture segmentation. Using gradient information to optimize (minimal sense) energy function, deformable areas are utilized to determine the contour of objects in an image [20]. The energy function E over the contour point c is used to define the generic ACM as presented in Eqn. (7).

$$E = \int_c \left(E_{img}(c) + \alpha E_{ext}(c) \right) dc \tag{7}$$

In equation (7), $\boldsymbol{E_{int}}$ stands for the internal energy that controls the form and length of the contour, $\boldsymbol{E_{img}}$ for the effects that alter the local portions, and $\boldsymbol{E_{ext}}$ for the object's past knowledge that controls the contour [38-40].

3.3 K-means Clustering

This technique of segmenting a picture into K clusters involves repetition. The goal of the vector quantization technique known as "k-means clustering," which has its roots in signal processing, is to divide a set of n observations into k clusters, each of which has as its prototype the observation with the closest mean.

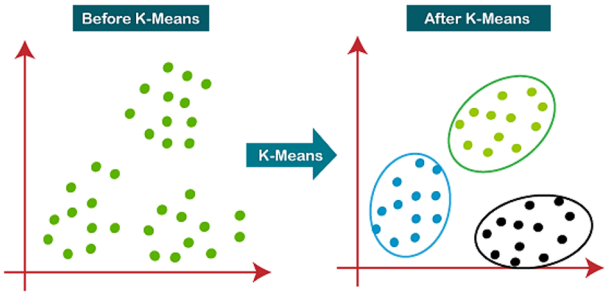

Fig. 4. K-means clustering process [30]

3.4 Graph Cuts

Graph cuts (G-cuts) is actually set of wide algorithms, where an image is conceptualized and to be structured as weighted undirected graph $G\ (V, E)$ by representing nodes V with pixels, weighted edges E with similarity (affinity) measured between nodes [20] i.e. $W: V^2 \rightarrow R^+$

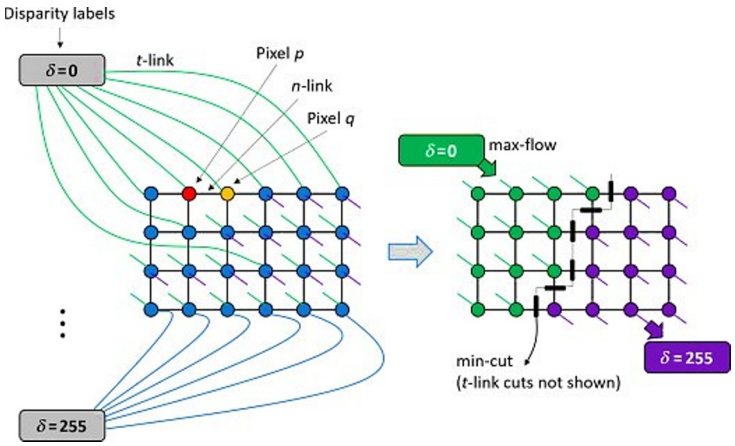

Fig. 4. Graph cut technique graphical illustration [33]

3.5 Nuclei Segmentation

Numerous authors have addressed the segmentation of nuclei using various conventional approaches, including mathematical morphology, pixel classification, level sets, and graph-based segmentation methods [19, 20, 24, 36], due to its crucial role in the automatic interpretation of stained tissue sections. While nucleus identification is often carried out by a spatially restricted convolutional neural network (SC-CNN), a new adjacent ensemble predictor (NEP) that is paired with CNN has been suggested to more reliably predict the class label of cell nuclei [25].

4 Detection of features

With the orientated fast and rotated brief (ORB) method, feature extraction and detection may be shown. The ORB effectively locates the picture's corners, whereas the fast component identifies features as regions of the image with a high difference in brightness. The most often used feature detection techniques are contouring, local binary pattern (LBP), and active localized contour model (LACM) [26-30, 31-34].

The nuclei segmentation is crucial for classification and grading accuracy. Segmentation and nuclei detection are important processes in the processing of histopathologic digital images [41-42]. The nuclei are crucial in and of themselves for assessing and verifying the presence of illness and the speed at which it spreads. A few of the feature detection techniques that have been employed successfully and efficiently are discussed in this study [33-43].

The centroid transform only works with binarized pictures and cannot be used to take advantage of addition cues since it identifies the seed points in the nucleus [20]. Shape-based detection uses calculations of side length and area to identify nuclei. Disorder D of distribution r, which is referred to as shape change, is mathematically defined as in Eqn. (8) Standard deviation and mean of r are σ_r and μ_r, respectively [15].

$$D(r) = 1 - \left(1 + \frac{\sigma_r}{\mu_r}\right)^{-1} \tag{8}$$

High computation is needed for circular shape-based nuclei identification by Hough transformation [20]. It is beneficial to increase accuracy by using a different technique to extract the feature from the critical areas. The structural, textural, and combination or hybrid techniques are intended to increase accuracy [17].

5 Classification methods from images

The data base makes it simple for the pathologist to make diagnostic and treatment judgements. The categorization of histology images is used nowadays. Because of their adaptability and successful outcomes, the majority of classifiers rely on support vector machine (SVM) and neural network (NN) classification techniques.

5.1 Support vector machine (SVM)

Laplace edge-based SVM classification that is compared to current applications. Figure (3) depicts the SVM classes' integration into features. The classifier can correctly detect other two kinds of cell nuclei with varied staining and scales in addition to the one type of nucleus pictures used to train it [12].

$$f(x) = \mathrm{sign}\left[\sum_{i=1}^{N} \alpha_i y_i K(x, x_i) + b\right] \tag{9}$$

Where $\boldsymbol{x}$ is the data point that has to be categorized, $\boldsymbol{x_i}$ is a support vector, N is the total number of support vectors, $\boldsymbol{b}$ is a constant used for training purposes, and $\boldsymbol{y_i}$ is the support vectors $\boldsymbol{x_i}$'s classified label. The Lagrengian multiplier is represented by the coefficients. In the instance of breast cancer, K is the kind of Kernel that specifically determines how the classifier classifies the nuclei; it does this by looking for malignant tissues by looking for nuclei.

The specified kernel function and its features determine the many sorts of kernels. The following are some of the most used kernel functions: Linear ($x_i^T x$), Polynomial $(x_i^T x + \tau)^d$, Radial Basis Function $\exp\left(-\frac{\left\|(x - x_i)^d\right\|^2}{2\sigma_i^2}\right)$ and Sigmoid $\tanh\left(k x_i^T x + \tau\right)$.

When utilizing a kernel-based SVM classifier, we must be very careful since the usage of the kernel function depends on the kind of application [8, 20-25].

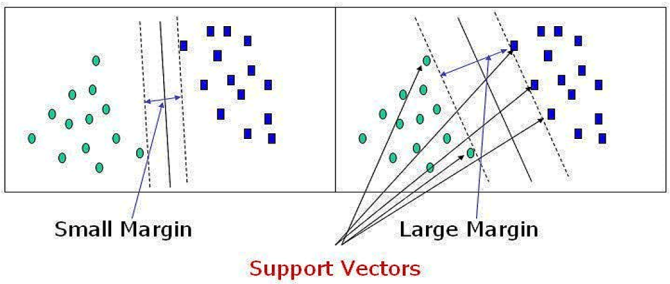

Fig. 3. Support vector machine (SVM) classifier with hyperplane representation [12]

A supervised model called the soft-max classifier (SMC) generalizes logistic regression as a function of selected samples $f_w(z) = \frac{1}{(1+e^{-w^T z})}$.

5.2 Convolutional Neural Network (CNN)

An input vector is mapped to an output vector using a convolutional neural network (CNN), which is made up of a series of functions or layers.

$$y = f(x;\, w_1, \ldots., w_L) = f_L(w_L)^\circ\, f_{L-1}(w_{L-1})^\circ \ldots.^\circ f_2(w_2)^\circ f_1(w_1) \qquad (10)$$

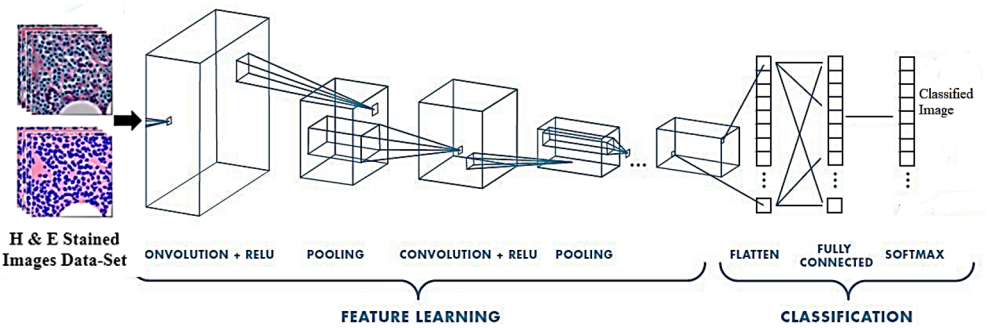

Fig. 4 Deep CNN network for image samples classification, having three main subparts (a) input image samples (b) feature extraction network and (c) fully connected neural network based classification [29].

The convolutional layer is a layer that multiplies pixels one by one using the kernel coefficients and the total of all the window's pixel values [35, 36, 42]. DCNN employs n x n unpadded convolutions with the specified kernel applied repeatedly, each convolution being followed by a rectified linear unit (ReLU) and a max pooling operation with a specific downsampling stride. The size of the kernel and its coefficients should be chosen depending on the application, for convolution, 3x3 or 5x5 order kernels are most often employed. The number of feature channels has to be doubled for each downsampling step. A 2x2 convolution (up-convolution) is all that is needed to simply reduce the number of channels needed at each stage of the expanding route. In order to make the network deeper, as illustrated in figure (4), the whole unit (convolution+ReLU+Max Pooling) is concatenated with the proportionally cropped feature map from the contracting, and the necessary number of convolutions with a certain kernel, followed by a ReLU. The loss of boundary pixels in each convolution necessitates cropping [26-35].

ReLU is a form of thresholding approach where the value of each pixel is either 0 or 1, and pooling is used to choose the pixel with the highest value or to take the average value of the window pixels. The window's dimensions should be chosen based on the need for precision. The act of flattening turns the pooled pixel matrix into a column matrix. The fully connected neural network is now receiving input from all of the column matrix pixels [36-40]. Now, we may get the categorized picture using the soft-max algorithm. Other existing neural networks are in use, like ResNet and U-Net, which are used specifically for segmenting biological images [30-37].

5.3 Training of deep learning network

The network is trained using stochastic gradient descent or any modified gradient descent approach using the input pictures and their related segmentation maps. The mathematical expression of the approximation function in Eqn. (11), which is dependent on activation [22-30].

$$f_k(x) = \frac{\exp(g_k(x))}{\sum_{k=1}^{N} \exp(g_k(x))} \tag{11}$$

Where $\boldsymbol{x} \in \boldsymbol{Q}$ and $\boldsymbol{Q}$ is the pixel matrix of an image, and $\boldsymbol{g_k(x)}$ is the activation in the kth feature channel at the pixel location. The approximate maximum function, $\boldsymbol{f_k(x)}$, is defined as follows: $\boldsymbol{f_k(x)} \approx \boldsymbol{1}$ for the class with the highest activation, and $\boldsymbol{f_k(x)} \approx \boldsymbol{0}$ for all other classes with the lowest activation. N is the number of classes. The departure of $\boldsymbol{f_{l(x)}(x)}$ from 1 is then penalised at each point using the following correlation by the cross entropy in Eqn. (12) [28].

$$E = \sum_{x \in x} w(x).\log\left(f_{l(x)}(x)\right) \tag{12}$$

Typically, 80% of the collection of pictures are used for training the network, while the remaining 20% are utilized for testing.

Table 2. Comparison of classification accuracy, feature extraction and detection methods

Ref. & Image Data-set	Object	Pre-processing method	Feature Extraction Method	Classifier Used	Classification Accuracy
H&E-stained coloured Images [15]	Cell Nuclei	Fourier shape discrimination	Contouring	Linear discriminant classifier (LDA)	77.00%
Microscopic biopsy images [14]	Cell Nuclei	Cascade Random Subspace ensembles scheme	Local Binary Pattern (LBP)	Support Vector Machine (SVM)	99.25%
Cell nucleus images [13]	Cell Nuclei	Sliding window to search through the image for nuclei	Quick edge detection or threshold	Support Vector Machine (SVM)	90.00%
Whole slide images [20]	Cell Nuclei	-	Morphological features	Support Vector Machine (SVM)	92.88% to 94.54%
Whole slide images [38]	Epithelial Nuclei (EN)	-	-	Simple linear iterative clustering (SLIC) algorithm	83.00%
H&E-stained Images [41]	Mitotic Cells	Adaptive Wiener filtering	Localized Active Contour Model (LACM)	A deep belief network	F-score of 84.29%
H&E-stained Images [42]	Stroma Cells	-	Local Binary Patterns (LBP)	Single- and multi-scale approaches	84.00%
H&E-stained Images [19]	Cell nuclei	Augmentation	Graph-Network	Binary class	99.47%

6 Performance parameters

On the basis of the performance parameters the used technics are discriminated, these parameters are-

$\text{Re}call = Sensitivity = TPR = \frac{TP}{TP+FN}$, $\text{Pr}ecision = \frac{TP}{TP+FN}$, Precision defines the closeness of classification. Recall is also defined as sensitivity, which shows the proportion of positive categories. $FPR = \frac{FP}{FP+TN}$, This defines the insensitivity or the proportion of false categories. Proportion of correct classification in all samples termed as accuracy. $Accuracy = \frac{TP+TN}{TP+FP+TN+FN}$ TP = True Positive, TN = True Negative, FN = False Negative FP = False Positive, TPR = True Positive Recall, FPR = False Positive Recall.

7 Conclusion

In this study, techniques for processing histopathological images are covered. Additionally, a comparison of picture classification and image detection techniques is given in table II, together with information on each method's performance. Researchers can more quickly and accurately create early detection techniques that may reduce the risk of breast cancer via screening according to the study and comparison analysis.

8 Future directions

The deep learning is very popular and effective approach for the detection and diagnosis of diseases. The combination of deep neural networks with popular machine learning (ML) techniques is attaining attention of researchers for designing improved performance systems. In future novel deep learning models can be designed for image segmentation by incorporating novel approaches related to feature fusion, edge aware, feature aware and region aware techniques. First of all, every learner must study about the basic concept of the deep learning, machine learning, and gain key concepts about the different layers. Generative adversarial network (GAN), autoencoder (AE), and segmentation networks are the popular deep learning models.

References

1. Breast Cancer Facts & Figures 2021-2022. *Atlanta: American Cancer Society*, Inc. (2021).
2. Breast Cancer report *WHO*, 2023. https://www.who.int/news-room/fact-sheets/detail/breast-cancer
3. B. Stenkvist, E. Bengtsson, E. T. Jarkrans, B Nordin, S Westman-Naeser "Histopathological systems of breast cancer classification: reproducibility and clinical significance" *J Clin Pathol 1983*, Vol-36, 392-398, (1983). http://jcp.bmj.com/
4. Y. X. Ci, T. Y. Gao, J. Feng, And Zhen Quan Guo "Fourier Transform Infrared Spectroscopic Characterization of Human Breast Tissue: Implications for Breast Cancer Diagnosis" *IEEE Transaction, Applied Spectroscopy* Volume 53, Number 3, (1999).
5. V. Ntziachristos and B. Chance "Probing physiology and molecular function using optical imaging: applications to breast cancer" *BioMed Central Ltd*. Print ISSN 1465-5411, Breast Cancer Research 2001, Vol-3 pp 41–46, (2001).
6. S. G. Vari, G. Brugal, R.D. Naber, G. Muller "Interactive Histopathology Consultation Network" *IEEE Transaction*, pp: 197-202, (2000).
7. S. G. Demos, R. Bold, R. D. White, and Rajendra Ramsamooj "Investigation of Near-Infrared Autofluorescence Imaging for the Detection of Breast Cancer" *IEEE journal of selected topics in quantum electronics*, vol. 11, (2005).
8. S. Waheed, R. A. Moffitt, Q. Chaudryl, A. N. Young, and M.D. Wang "Computer Aided Histopathological Classification of Cancer Subtypes" *IEEE conference* pp:503-508, (2007).

9. M. N. Gurcan, L. E. Boucheron, A. Can, A. Madabhushi, S. Nasir, M. Rajpoot, and B. Yener "Histopathological Image Analysis: A Review" *IEEE reviews in biomedical engineering*, vol. 2, pp: 147-169, (2009).
10. H. Sung, P. S. Rosenberg et.al "Female Breast Cancer Incidence Among Asian and Western Populations: More Similar Than Expected" *JNCI J Natl Cancer Inst*, April-13, (2015), doi:10.1093/jnci/djv107.
11. Y. A. Kofahi, W. Lassoued, W. Lee, and B. Roysam "Improved Automatic Detection and Segmentation of Cell Nuclei in Histopathology Images" *IEEE Transactions on Biomedical Engineering*, vol. 57, pp: 841-852, (2010).
12. P Pandit, R Patil et.al "Prevalence of Molecular Subtypes of Breast Cancer: A Single Institutional Experience of 2062 Patients" *Eur J Breast Health*; pp: 39-43, (2020). DOI: 10.5152/ejbh.2019.4997
13. J. W. Han, T. P. Breckon, D. A. Randell, G. Landini "The application of support vector machine classification to detect cell nuclei for automated microscopy" *Journal on Machine Vision and Applications*, Springer-05 Jan, (2010). DOI 10.1007/s00138-010-0275-y
14. Y. Zhang, B. Zhang, F. Coenen, W. Lu "Breast cancer diagnosis from biopsy images with highly reliable random subspace classifier ensembles" *International Journal in Machine Vision and Applications,* Springer-17 September (2012), DOI:10.1007/s00138-012-0459-8.
15. S. Kothari, J. H. Phan, A. N. Young and M. D. Wang "Histological image classification using biologically interpretable shape-based features" *BMC Medical Imaging*, pp:3-16, (2013), http://www.biomedcentral.com/1471-2342/13/9.
16. S. Krishnamurthy, K. Mathews, S. McClure, M. Murray "Multi-Institutional Comparison of Whole Slide Digital Imaging and Optical Microscopy for Interpretation of Haematoxylin-Eosin–Stained Breast Tissue Sections" *Arch Pathol Lab Med*—vol 137, December (2013), doi: 10.5858/arpa.2012-0437-OA.
17. E. Ozdemir and C. G. Demir "A Hybrid Classification Model for Digital Pathology Using Structural and Statistical Pattern Recognition" *IEEE Transactions on Medical Imaging*, February 2013, Vol. 32, No. 2, (2013).
18. L. Alzubaidi *et al.*, Review of deep learning: concepts, CNN architectures, challenges, applications, future directions, vol. 8, no. 1. *Springer International Publishing*, 2021. doi: 10.1186/s40537-021-00444-8.
19. V. Patel, V. Chaurasia, R. Mahadeva, and S. P. Patole, "GARL-Net: Graph Based Adaptive Regularized Learning Deep Network for Breast Cancer Classification," *IEEE Access*, vol. 11, no. January, pp. 9095–9112, (2023), doi: 10.1109/ACCESS.2023.3239671.
20. H. Irshad, A. Veillard, L. Roux, and D. Racoceanu "Methods for Nuclei Detection, Segmentation, and Classification in Digital Histopathology: A Review—Current Status and Future Potential" *IEEE Reviews in Biomedical Engineering*, vol. 7, (2014).
21. A. K. Itawadiya, R. Mahle, V. Patel, and D. Kumar, "Design a DSP operations using vedic mathematics," *Int. Conf. Commun. Signal Process. ICCSP 2013 - Proc.*, pp. 897–902, (2013), doi: 10.1109/iccsp.2013.6577186.
22. R. Mahadeva, M. Rathore, V. Chaurasia, M. Shandilya, S. P. Patole, and V. Patel, "Edge Detection and Color Mapping Based Diabetic Retinopathy from Fundus Images," *1st IEEE Int. Conf. Innov. High Speed Commun. Signal Process. IHCSP 2023*, pp. 483–487, (2023), doi: 10.1109/IHCSP56702.2023.10127198.
23. R. Mahadeva, S. P. Patole, V. Patel, V. Chaurasia, A. Sharma, and R. Sharma, "Deep Transfer Learning with Multi-Level Features Extraction Approach for Breast Cancer Classification," *1st IEEE Int. Conf. Innov. High Speed Commun. Signal Process. IHCSP 2023*, pp. 471–474, (2023), 10.1109/IHCSP56702.2023.10127180.
24. S. Bhardwaj, V. Chaurasia, E. Ahmad Siddiqui, V. Patel, A. Sharma, and M. Tiwari, "Feature Extraction Based Domain Kickout Method for Fractal Image Compression," *1st IEEE Int. Conf. Innov. High Speed Commun. Signal Process. IHCSP 2023*, no. i, pp. 514–518, (2023), doi: 10.1109/IHCSP56702.2023.10127206.
25. L. Sun, J. Zhang, W. Ding, and J. Xu, "Feature reduction for imbalanced data classification using similarity-based feature clustering with adaptive weighted K-nearest neighbors," *Inf. Sci. (Ny).*, vol. 593, pp. 591–613, (2022), doi: 10.1016/j.ins.2022.02.004.
26. S. Pouyanfar *et al.*, "A survey on deep learning: Algorithms, techniques, and applications," *ACM Comput. Surv.*, vol. 51, no. 5, (2018), doi: 10.1145/3234150.
27. S. Panigrahi, A. Nanda, and T. Swarnkar, "A Survey on Transfer Learning," *Smart Innov. Syst. Technol.*, vol. 194, no. 10, pp. 781–789, (2021), doi: 10.1007/978-981-15-5971-6_83.
28. R. Mahadeva, M. Kumar, V. Gupta, G. Manik, and S. P. Patole, "Modified Whale Optimization Algorithm based ANN: a novel predictive model for RO desalination plant," *Sci. Rep.*, vol. 13, no. 1, pp. 1–14, (2023), doi: 10.1038/s41598-023-30099-9.
29. R. Mahadeva, M. Kumar, S. P. Patole, and G. Manik, "Desalination Plant Performance Prediction Model Using Grey Wolf Optimizer Based ANN Approach," *IEEE Access*, vol. 10, pp. 34550–34561, 2022, doi: 10.1109/ACCESS.2022.3162932.
30. A. Goel, R. Mahadeva, and G. Manik, "Analysis and Optimization of Parabolic Trough Solar Collector to Improve Its Optical Performance," *J. Sol. Energy Eng. Trans. ASME*, vol. 145, no. 3, pp. 1–12, (2023), doi: 10.1115/1.4055995.
31. R. Mahadeva, M. Kumar, S. P. Patole, and G. Manik, "Employing artificial neural network for accurate modeling, simulation and performance analysis of an RO-based desalination process," *Sustain. Comput.*

Informatics Syst., vol. 35, no. April, p. 100735, (2022), doi: 10.1016/j.suscom.2022.100735.

32. R. Mahadeva, M. Kumar, G. Manik, and S. P. Patole, "Modeling, simulation, and optimization of the membrane performance of seawater reverse osmosis desalination plant using neural network and fuzzy based soft computing techniques," *Desalin. Water Treat.*, vol. 229, pp. 17–30, (2021), doi: 10.5004/dwt.2021.27386.
33. M. Veta, J. P. W. Pluim, P. J. van Diest, and Max A. Viergever "Breast Cancer Histopathology Image Analysis: A Review" *IEEE Transactions on Biomedical Engineering*, Vol. 61, No. 5, (2014).
34. F. A. Spanhol, L. S. Oliveira, C. Petitjean, Laurent Heutte "A Dataset for Breast Cancer Histopathological Image Classification" DOI 10.1109/TBME.2015.2496264, *IEEE Transactions on Biomedical Engineering*, (2015).
35. M. Tiwari, V. Chaurasia, E. A. Siddiqui, V. Patel, A. Kumar, and M. Patankar, "Enhanced Image Compression Using Fractals and Principle Component Analysis," *1st IEEE Int. Conf. Innov. High Speed Commun. Signal Process. IHCSP 2023*, no. 2, pp. 502–507, (2023), doi: 10.1109/IHCSP56702.2023.10127168.
36. R. Mahadeva, M. Kumar, S. P. Patole, and G. Manik, "PID Control Design Using AGPSO Technique and Its Application in TITO Reverse Osmosis Desalination Plant," *IEEE Access*, vol. 10, no. November, pp. 125881–125892, (2022), doi: 10.1109/ACCESS.2022.3224127.
37. R. Mahadeva, M. Kumar, A. Goel, S. P. Patole, and G. Manik, "A Novel AGPSO3-based ANN Prediction Approach: Application to the RO Desalination Plant," *Arab. J. Sci. Eng.*, (2023), doi: 10.1007/s13369-023-07631-0.
38. B. E. Bejnordi, M. Balkenhol, G. Litjens "Automated Detection of DCIS in Whole-Slide H&E Stained Breast Histopathology Images" *IEEE Transactions on Medical Imaging*, vol. 35, September (2016).
39. K. Sirinukunwattana, S. E Ahmed Raza, Y.W. Tsang "Locality Sensitive Deep Learning for Detection and Classification of Nuclei in Routine Colon Cancer Histology Images" *IEEE Transactions on Medical Imaging*, May 2016, Vol. 35, (2016).
40. J. Xu, L. Xiang, Q. Liu, H. Gilmore, J. Wu, J. Tang "Stacked Sparse Autoencoder (SSAE) for Nuclei" *IEEE Transactions on Medical Imaging*, January 2016, vol. 35, (2016).
41. B. E. Bejnordi, G. Litjens, N. Timofeeva, I. O. Holle "Stain Specific Standardization of Whole-Slide Histopathological Images" *IEEE Transactions on Medical Imaging*, February 2016, vol. 35, (2016).
42. S. Reis, P. Gazinska etc.al "Automated Classification of Breast Cancer Stroma Maturity from Histological Images" *IEEE transactions on biomedical engineering*, October 2017, vol. 64, no. 10, (2017).
43. S. Sheikh, B. Suthar, and M. Uddin, in 2017 International Conference on Innovations in Control, Communication and Information Systems (ICICCI) (IEEE, 2017), pp. 1–6